NANO LETTERS

XXXX
Vol. xx, No. x
-

Converse Piezoelectric Effect Induced Transverse Deflection of a Free-Standing ZnO Microbelt

Youfan Hu, Yifan Gao, Srikanth Singamaneni, Vladimir V. Tsukruk, and Zhong Lin Wang*

School of Material Science and Engineering, Georgia Institute of Technology, Atlanta, Georgia 30332-0245

Received April 6, 2009; Revised Manuscript Received June 1, 2009

ABSTRACT

We demonstrate the first electric field induced transverse deflection of a single-crystal, free-standing ZnO microbelt as a result of converse piezoelectric effect. For a microbelt growing along the *c*-axis, a shear stress in the *a*-*c* plane can be induced when an electric field *E* is applied along the *a*-axis of the wurtzite structure. As amplified by the large aspect ratio of the microbelt that grows along the *c*-axis, the strain localized near the root can be detected via the transverse deflection perpendicular to the ZnO microbelt. After an experimental approach was carefully designed and possible artifacts were ruled out, the experimentally observed degree of deflection of the microbelt agrees well with the theoretically expected result. The device demonstrated has potential applications as transverse actuators/sensors/switches and electric field induced mechanical deflectors.

Nanodevices made using one-dimensional (1D) nanostructures such as nanowires and nanobelts are largely based on longitudinal 1D nanostructures that are confined in diameter dimension, in which the axial transport property is the dominant process for building various nanodevices for nanoelectronics, nanosensors, nanoLED, nanolasers, and nanosolar cell.[1−7] ZnO nanowires (NWs) and nanobelts (NBs) are the dominant oxide 1D nanomaterials that have been widely studied. Owing to the unique piezoelectric and semiconducting coupled properties, various innovative piezotronic devices have been fabricated based on ZnO NWs, such as nanogenerators,[8−12] piezoelectric field effect transistors,[13] strain sensors[14] and optoelectronic sensors,[15] etc. As for transducers, the most common configuration for ZnO is to use the axial directional deformation of the NWs when an electric potential is applied along its length, because the *c*-axis has the largest converse piezoelectric coefficient. There are few examples about utilization of the converse piezoelectric effect for inducing transverse mechanical deflection of a NW/NB, in which the mechanical action is perpendicular to the nanowire/nanobelt. A common design is that such a device requires a nonsymmetric, side-by-side bilayer nanowire shape structure (such as ZnO/Al_2O_3 for example) that has distinctly different piezoelectric properties, so that the electrical response of the two would result in different degrees of axial deformation, which lead to the transverse deflection of the nanowire. This is similar to the design of a thermal meter based on two materials that have different thermal expansion coefficients.

In this paper, we demonstrate the first electric field induced transverse deflection of a single-crystal, free-standing ZnO microbelt as a result of converse piezoelectric effect without utilizing a nonsymmetric bilayer structure. After an experimental approach was carefully designed and possible artifacts were ruled out, the experimentally observed degree of deflection of the microbelt agrees well with the theoretically expected result. The device has potential applications as transverse actuators/sensors/switches and electric field induced mechanical deflectors.

From a structure point of view, wurtzite zinc oxide has a hexagonal structure (space group C_{6v}) with lattice parameters $a = 0.3296$ and $c = 0.52065$ nm. The structure of ZnO can be simply described as a number of alternating planes composed of tetrahedral coordinated O^{2-} and Zn^{2+} ions, stacked alternatively along the *c*-axis. The tetrahedral coordination in ZnO results in noncentral symmetric structure and, consequently, the piezoelectricity and pyroelectricity. Another important characteristic of ZnO is the polar surfaces. The most common polar surface is the basal plane. The oppositely charged ions produce positively charged Zn-(0001) and negatively charged O-$(000\bar{1})$ surfaces. This means that $+c$ and $-c$ are nonsymmetric. An important feature of the wurtzite structure is the piezoelectric coupling between the *a*-axis and *c*-axis through e_{31} and e_{15}. Through e_{31}, a normal straining along the *a*-axis is able to result in *c*-axis

* To whom correspondence should be addressed, zlwang@gatech.edu.

10.1021/nl901102k CCC: $40.75 © XXXX American Chemical Society

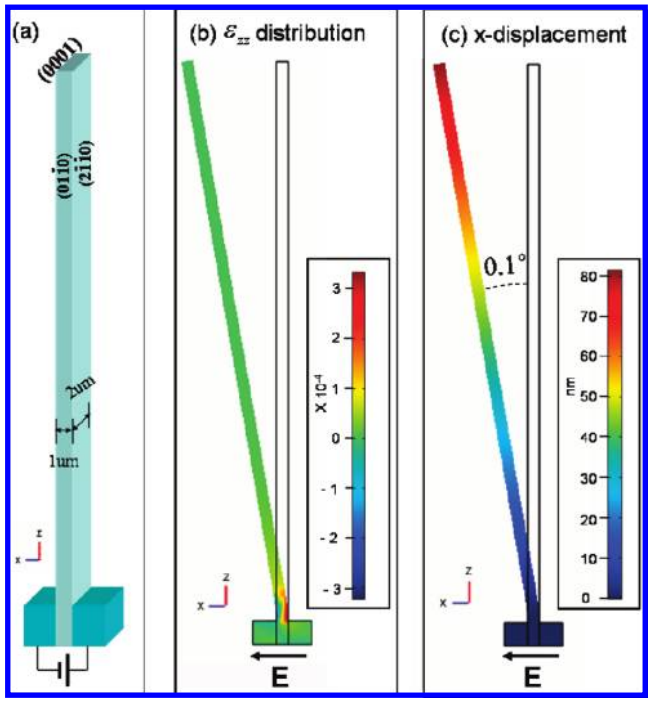

Figure 1. (a) Schematic diagram showing the design of the device. The calculated corresponding displacements and strain in the microbelt in responding to an applied electric field perpendicular to the *c*-axis: (b) ε_{zz}distribution and (c) displacement along the *x*-direction. The deformations in (b, c) were enlarged 100× times in the *x*-direction for illustration purposes.

directional piezoelectric field; through e_{15}, a shear strain in the $a-c$ plane will result in a piezoelectric field along the *a*-axis. As for the converse piezoelectric effect, with the nonsymmetric structures along $+c$ and $-c$ owing to the tetrahedral coordination, different straining can be induced in the $a-c$ plane if an electric field is applied along the *a*-axis.

The above discussion can be made quantitative with the assistance of numerical simulation. The setup of our simulation model is presented in Figure 1a. The possible growth direction of the nano-/microbelt can be either [0001], [01$\bar{1}$0], or [2$\bar{1}\bar{1}$0].[16,17] We choose the belt with a growth direction along the *c*-axis [0001], and thus the side surfaces should be (2$\bar{1}\bar{1}$0) and (01$\bar{1}$0). The dimension of the belt is 50 μm in length, and with a rectangular cross section of 1 μm × 2 μm. Two electrodes are built respectively adjacent to the (2$\bar{1}\bar{1}$0) side surfaces of a free-standing microbelt at the root, but they are insulated from the belt so that there is no electric current being transported across the belt. The applied voltage is to create an electric field in the ZnO microbelt. Our theoretical calculation is based on a static model, and the details of the simulation can be found elsewhere.[18] When we consider the C_{6v} symmetry of the wurtzite structured ZnO crystal, and after the so-called Voigt (or Nye) two-index notation[19] is used to keep the notation compact, the constitutive equations can be rewritten as

$$\begin{cases} \sigma_p = c_{pq}\varepsilon_q - e_{kp}E_k \\ D_i = e_{iq}\varepsilon_q + \kappa_{ik}E_k \end{cases} \quad (1)$$

where σ is the stress, ε is the strain, $\vec{E}$ is the electric field, and $\vec{D}$ is the electric displacement. For simplicity of illustrating the physical model, we assume that the doping level in ZnO is rather low so that the free charge carriers in the volume can be ignored, which greatly simplifies the numerical calculation. We can utilize the finite element method (FEM) to calculate the response of a ZnO belt to an electric field applied perpendicular to the *c*-axis. The mechanical property of ZnO is $E = 129.0$ GPa and $\nu = 0.349$,[18] the relative dielectric constants are $\kappa_{11} = 7.77$ and $\kappa_{33} = 8.91$ for bulk ZnO,[20] and the piezoelectric constants are $e_{31} = -0.51$ C/m^2, $e_{33} = 1.22$ C/m^2, and $e_{15} = -0.45$ C/m^2.[21] A voltage of +100 V is applied uniformly through the two electrodes along the *x*-direction across the width of the microbelt. In the simulation, the two outer surfaces of the two electrodes perpendicular to the *x*-axis are set to be mechanical fixed, but all of the other surfaces and boundaries are free to relax/move to a mechanical equilibrium state.

First, when a voltage of 100 V is applied along the *x*-direction ($\vec{E} = E_1\hat{i}$), according to eq 1, the converse piezoelectric effect will introduce a shear stress in the $x-z$ plane (e.g., $a-c$ plane) owing to e_{15} coupling, which results in a ε_{zz} component that is distributed as shown in Figure 1b. The strain concentrates at the bottom of the belt near the electrodes, changing from tensile into compressive along the direction of the electric field. The effect of the shear strain is equivalent to applying a force in the $x-z$ plane, which at least has a component that is perpendicular to the nanobelt. The force decays with the increase of the distance from the nanobelt root, but a small torque is created in the $x-z$ plane. The microbelt has a high flexibility, and the strain at the root of the belt introduces a bending, resulting in a lateral deflection along the *x*-direction, as shown in Figure 1c, in which the deflection of the microbelt has been magnified by 100× to visually illustrate the effect. Although, the strain directly induced by the converse piezoelectric effect is small, the transverse deflection is amplified by the large aspect ratio of the microbelt. In our model, the 50 μm long belt has a maximal transverse deflection of 80 nm at the top. In fact, the practical belt has much higher aspect ratio. The length could extend to several millimeters. Thus, the resulting *x*-displacement could be close to 1 μm. The deflection angle of the microbelt has been calculated to be 0.1°, which does not depend on the actual length of the belt. We will use this deflection angle to quantify our experimental results. Finally, it should be mentioned that from the simulations for different applied voltages, we find that there is a linear relationship between the deflection angle and the applied voltage. Also, when the applied voltage changes its sign, the deflection will change its direction.

The device structure and the experimental design for measuring the converse piezoelectric effect are presented in Figure 2. The ZnO microbelts used in our study were grown by a vapor−solid process as described earlier.[15] First, an individual mirobelt was placed at the edge of a silicon wafer covered with 200 nm Si_3N_4. The end of the belt on the wafer was pasted with poly(dimethylsiloxane) (PDMS) to be fixed on the substrate, but the other end was free-standing. Then, another silicon wafer covered with Si_3N_4 was bonded. The

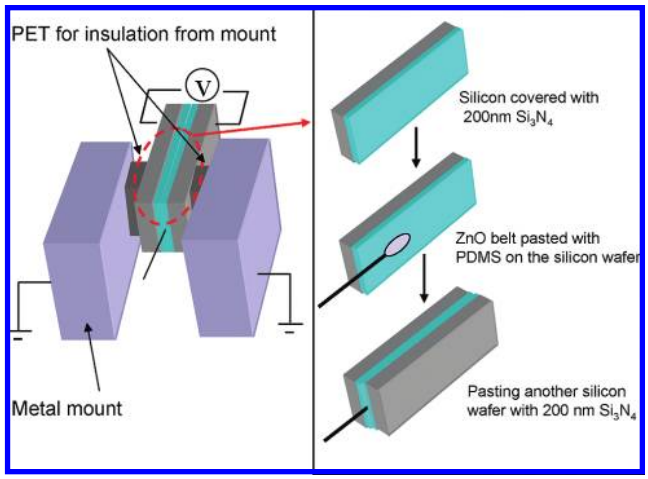

Figure 2. Schematic diagram about the structure of the device and the experimental measurement setup. The right part shows the fabrication process of the device.

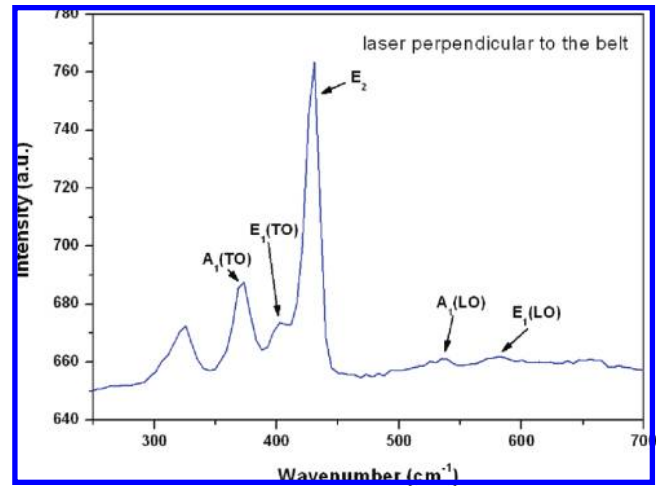

Figure 3. Raman spectrum taken from the ZnO microbelt used for fabricating the device. The laser beam was perpendicular to the belt. The five marked peaks indicate the belt grow along the *c*-axis.

silicon wafer worked as electrodes, while the Si_3N_4 and PDMS kept the belt insulated from the electrodes. During the measurement, the total device was affixed to a grounded scanning electron microscopy (SEM) "U" shape metal mount. A thin layer of poly(ethylene terephthalate) (PET) was put between the device and the mount to ensure insulation. The split mount worked as a "Faraday cage" to screen the belt and also kept it away from various perturbations from environment, such as air flow.

Confocal Raman microscopy was employed to identify the growth orientation of the ZnO microbelt without destructing the as-made device.[22] This has been demonstrated as a powerful technique for identifying the crystallographic orientation of a nanobelt without destructing the sample. On the basis of the selection rules established for ZnO, when the incident light is perpendicular to the *c*-axis of the ZnO belt, the Raman spectrum will consist of E_2 (438 cm^{-1}), A_1(TO) (380 cm^{-1}), E_1(TO) (410 cm^{-1}), A_1(LO) (548 cm^{-1}), and E_1(LO) (583 cm^{-1}).[23] A Witec (Alpha 300R) confocal Raman microscope was used to carry out the Raman characterization. The excitation source was an Ar^+ ion laser with a wavelength of 514.5 nm. Figure 3 is the Raman spectrum taken from a microbelt used in a fabricated device. The five marked peaks clearly indicated that the growth direction of the belt is along the *c*-axis. After its orientation was confirmed, this device was introduced into the scanning electron microscope chamber to conduct the converse piezoelectric experiments.

Figure 4a is an SEM image of the device. A microbelt sticks out from the interface of two attached Si wafers. The inset is a higher magnification image taken from the circled area. The cross-section size of this belt is about 2 μm × 4 μm. Putting this parameter into our simulation model, we can get a deflection angle of 0.05° when a +100 V voltage is applied. A four-probe system was utilized in the SEM chamber to apply the electric field. The *x*-direction displacement is most significant at the tip of the belt, so we focused on this part for capturing the deflection. The results are shown in Figure 4b. The displacements in responding to +100 and

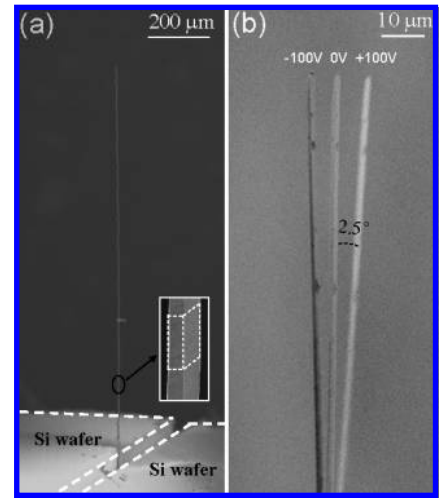

Figure 4. (a) SEM image of the device without applying an external voltage. Inset: higher magnification image taken from the circled part, showing a rectangular cross section. (b) Superimposed SEM images recorded when voltages of −100, 0, and +100 V, respectively, were applied across the width of the microbelt at its root. The large deflection was created mainly by static charging effect, although there was contribution from the conversing piezoelectric effect (see text for details).

−100 V are almost equal, but with opposite deflection directions. It appears that this might be the phenomenon we had expected, but it should be notice that the deflection angle of 2.5° is much larger than the deflection angle expected from simulation. In our device design, the ZnO belt was insulated from the environment. When we conducted our experiment in the SEM, the irradiation of the electron beam introduced a charging up effect to the ZnO microbelt. Therefore, the strong electrostatic attraction between the charged ZnO belt and the applied electric field contributed to a large extent to the observed deflection. In order to eliminate this surface charging effect, we took out our device from the SEM chamber and use an optical microscope equipped with a CCD to record the related experiment results.

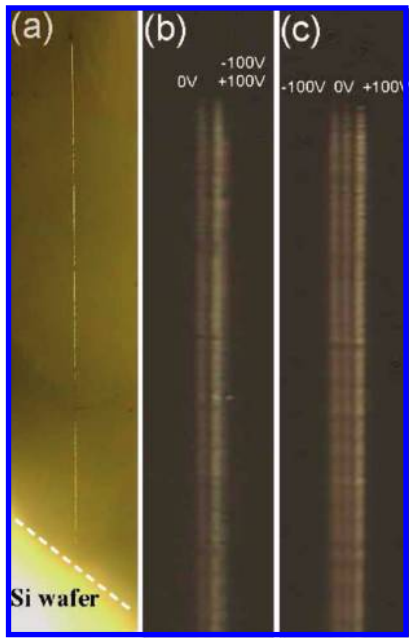

Figure 5. (a) Optical image of the device without applying a voltage. Deflection in responding to applying ±100 V (b) before and (c) after Au coating across the width of the microbelt.

The optical image of the device is shown in Figure 5a. Before every measurement, the belt was grounded by a needle to eliminate surface charges. At first, when +100 and −100 V voltages were applied, we received the same direction of deflection with almost equal magnitude, as shown in Figure 5b. Although there was no surface charging effect in this case, the electrostatic induction under the applied potential introduced static charges in the belt with different signs at opposite ends of the belt. The top end always had the same sign of charges as the electrode at which the voltage was applied to (the other electrode is grounded), because the electrode was located at the root of the belt. So there was a constant repulsive force between the electrode and the tip of the belt. When we switched the electrode to apply a voltage, the deflection correspondingly changed its direction. In order to eliminate this effect, we sputtered a thin layer of Au (15 nm) on the surface of the belt at its free-standing part (upper part away from the root). It was thin and will not change the mechanical properties of the belt significantly. But it was enough to screen the free-standing part of the belt from electrostatic charging. Then we carried out measurement again under an optical microscope, and the results are shown in Figure 5c. The deflections were almost equal magnitude but with opposite deflection directions responding to the applied +100 and −100 V, respectively. The absolute magnitude was reduced a bit after Au coating. The deflection angle was measured to be ∼0.18°. The physical parameters we used in our simulation were all from the bulk ZnO material, the actual electromechanical response should be a little larger than the simulated result in the microsystem, because the piezoelectric coefficient for a nanobelt was found to increase with the reduction in size[24] possibly due to surface effect and dislocation free volume.[16] Considering all of the above facts, the experimental deflection angle is reasonably consistent with our calculated result. We

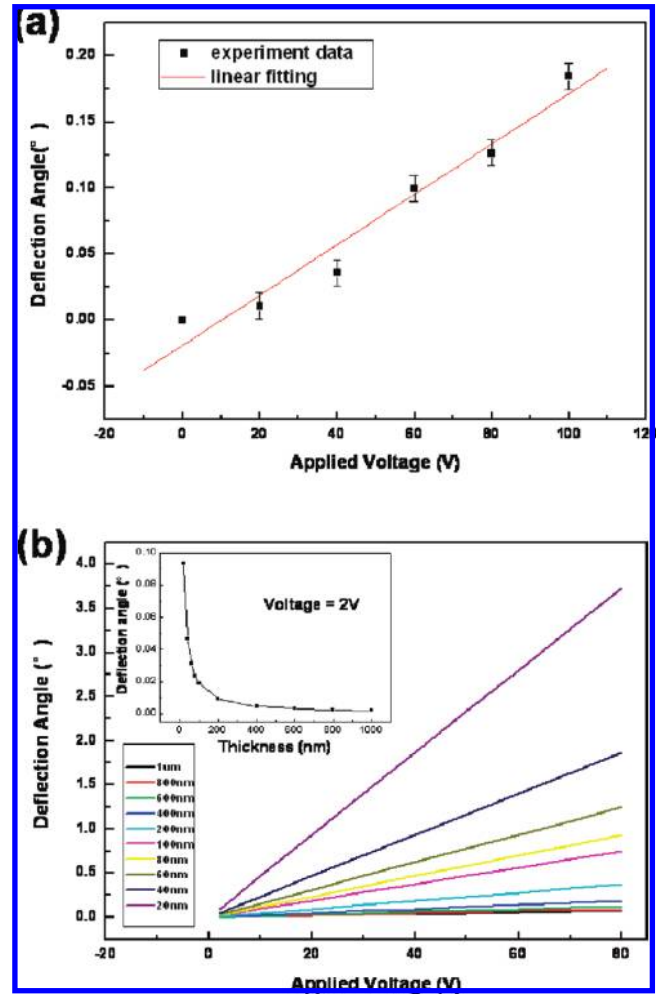

Figure 6. Transverse deflection angle of a microbelt as a voltage was applied across its width, showing a linear relationship. (b) Simulated results to predict the trend of the measured deflection angle as a function of nanobelt width and the applied voltage. The inset is the calculated deflection angle as a function of nanobelt width at a fixed applied voltage of 2 V across its width, showing the drastic increase in deflection angle in the nanobelt is thinner than 100 nm.

also measured the deflections corresponding to different applied voltage; a linear relationship was received, as shown in Figure 6a.

To extrapolate the results shown in Figure 6a to nanoscale, we have calculated the degree of belt bending as a function of its size and the applied voltage, as shown in Figure 6b. It is obvious that, when the width of the belt reduces, the slope of the deflection angle−applied voltage curve increases quickly, indicating the high sensitivity of the nanobelt to converse piezoelectric effect. As indicated in the inset of Figure 6b, when the applied voltage is kept at 2 V, the deflection angle reaches ∼0.1° as the width reduces to 20 nm. With this low level voltage range, this transverse deflection can have a more practical application. But the manipulation of the nanobelt at nanoscale is usually carried out in SEM. The charging up effect could strongly affect the measured results. Caution must be exercised to rule out possible artifacts.

In conclusion, when an electric field is applied perpendicular to a ZnO belt that has a growth direction of the *c*-axis, the converse piezoelectric effect creates a shear stress in the *a*-plane, resulting in a bending of the free-standing belt, and transfers this tiny deformation at the root into a much larger transverse displacement due to the large aspect ratio of the belt. This transverse deflection has been observed experimentally for the first time, and the experimental data agree well with the theoretically calculated results. The device has potential applications as transverse actuators/sensors/switches and electric field induced mechanical deflectors.

Acknowledgment. Research supported by DARPA (Army/AMCOM/REDSTONE AR, W31P4Q-08-1-0009), BES DOE (DE-FG02-07ER46394), Air Force Office (FA9550-08-1-0446), DARPA/ARO W911NF-08-1-0249, KAUST Global Research Partnership, World Premier International Research Center (WPI) Initiative on Materials Nanoarchitectonics, MEXT, Japan, and NSF (DMS 0706436, CMMI 0403671).

References

(1) Lu, W.; Xie, P.; Liber, C. M. *IEEE Trans. Electron Devices* **2008**, *55*, 2859–2876.
(2) Patolsky, F.; Timko, B. P.; Zheng, G.; Lieber, C. M.; Lundstrom, M. *MRS Bull.* **2007**, *32*, 142–149.
(3) Tian, B.; Kempa, T. J.; Lieber, C. M. *Chem. Soc. Rev.* **2009**, *38*, 16–24.
(4) Tian, B.; Zheng, X.; Kempa, T. J.; Fang, Y.; Yu, N.; Yu, G.; Huang, J.; Lieber, C. M. *Nature* **2007**, *449*, 885–889.
(5) Law, M.; Greene, L. E.; Johnson, J. C.; Saykally, R.; Yang, P. *Nature* **2005**, *4*, 455–459.
(6) Wang, Z. L. *Mater. Sci. Eng., R* **2009**, *64*, 3–4.
(7) Wang, Z. L. *J. Nanosci. Nanotechnol.* **2008**, *8*, 27–55.
(8) Wang, Z. L.; Song, J. H. *Science* **2006**, *312*, 242–246.
(9) Wang, X. D.; Song, J. H.; Liu, J.; Wang, Z. L. *Science* **2007**, *316*, 102–105.
(10) Qin, Y.; Wang, X. D.; Wang, Z. L. *Nature* **2008**, *451*, 809–813.
(11) Yang, R. S.; Qin, Y.; Dai, L. M.; Wang, Z. L. *Nat. Nanotechnol.* **2009**, *4*, 34–39.
(12) Yang, R. S.; Qin, Y.; Li, C.; Zhu, G.; Wang, Z. L. *Nano Lett.* **2009**, *9*, 1201–1205.
(13) Wang, X. D.; Zhou, J.; Song, J. H.; Liu, J.; Xu, N. S.; Wang, Z. L. *Nano Lett.* **2006**, *6*, 2768–2772.
(14) Zhou, J.; Gu, Y. D.; Fei, P.; Mai, W. J.; Gao, Y. F.; Yang, R. S.; Bao, G.; Wang, Z. L. *Nano Lett.* **2008**, *8*, 3035–3040.
(15) Gao, P.; Wang, Z. Z.; Liu, K. H.; Xu, Z.; Wang, W. L.; Bai, X. D.; Wang, E. G. *J. Mater. Chem.* **2009**, *19*, 1002–1005.
(16) Pan, Z. W.; Dai, Z. R.; Wang, Z. L. *Science* **2001**, *291*, 1947–1949.
(17) Kong, X. Y.; Wang, Z. L. *Nano Lett.* **2003**, *3*, 1625–1631.
(18) Gao, Y. F.; Wang, Z. L. *Nano Lett.* **2007**, *7*, 2499–2505.
(19) Nye, J. F. *Physical Properties of Crystals*; Oxford University Press: Oxford, 1957.
(20) Ashkenov, N.; Mbenkum, B. N.; Bundesmann, C.; Riede, V.; Lorenz, M.; Spemann, D.; Kaidashev, E. M.; Kasic, A.; Schubert, M.; Grundmann, M.; Wagner, G.; Neumann, H.; Darakchieva, V.; Arwin, H.; Monemar, B. *J. Appl. Phys.* **2003**, *93*, 126–133.
(21) Carlotti, G.; Socino, G.; Petri, A.; Verona, E. *Appl. Phys. Lett.* **1987**, *51*, 1889–1891.
(22) Singamaneni, S.; Gupta, M.; Yang, R. S.; Tomczak, M. L.; Naik, R.; Wang, Z. L.; Tsukruk, V. V., to be submitted.
(23) Ozgur, U.; Alivov, Y.; Liu, C.; Teke, A.; Reshchikov, M. A.; Dogan, S.; Avrutin, V.; Cho, S. J.; Morkoc, H. *J. Appl. Phys.* **2005**, *98*, 041301.
(24) Zhao, M. H.; Wang, Z. L.; Mao, S. X. *Nano Lett.* **2004**, *4*, 587–590.

NL901102K